

Flexible Free-Standing VO₂(B) Nanobelt Films as Additive-Free Cathode for Lithium-Ion Batteries

Jijiang Huang¹, Xiaofei Wang¹, Junfeng Liu^{1,*}, Xiaoming Sun¹, Li Wang^{2,*} and Xiangming He²

¹ State Key Laboratory of Chemical Resource Engineering, Beijing University of Chemical Technology, Beijing 100029, China;

² Institute of Nuclear & New Energy Technology, Tsinghua University, Beijing 100084, PR China

*E-mail: ljf@mail.buct.edu.cn ; wang-l@tsinghua.edu.cn

Received: 7 March 2011 / Accepted: 8 April 2011 / Published: 1 May 2011

Flexible free-standing VO₂(B) nanobelt films were designed as additive-free cathode for lithium ion batteries, via self-assembly of VO₂(B) nanobelts with a filtration technology. VO₂(B) nanobelts with different size were prepared by hydrothermal reaction with various amount of formic acid addition. The phase structure and morphology were analyzed by X-ray diffraction and scanning electron microscopy, which revealed high crystallinity and homogeneous morphology. A constant current charge-discharge test was employed to investigate the electrochemical properties. These films exhibited initial specific capacity of 219.4 mAh/g at current density of 10mA/g in the voltage range 4.0–1.5V vs. Li⁺/Li. Distinct voltage plateaus around 2.5V were observed, which was seldom reported. The size effect of the materials on electrochemical performance was investigated and the results demonstrated that the electrochemical performance of the VO₂(B) nanobelts is significantly impacted by their size.

Keywords: Nanobelts, vanadium dioxide, lithium-ion batteries, additive-free, free-standing

1. INTRODUCTION

In recent years, rechargeable lithium ion batteries have attracted significant attention at both fundamental and applied levels because of their high energy density and design flexibility.[1-8] In the field of cosmetics and medicines, new technologies such as iontophoresis, compact and lightweight electrical sources are needed.

Ultra-thin soft batteries have met this demand by offering shape versatility and flexibility.[9] Nanotechnology brings new opportunities to this area and many efforts have been devoted to

fabricating one-dimensional nanostructured materials to improve the battery performance. For instance, carbon nanotubes (CNTs) were utilized in batteries to impart mechanical flexibility and to improve the structural and electrochemical properties.[10-12] Recently, CNTs have been embedded in cellulose to produce paper-like flexible batteries and capacitors.[13] On the other hand, additive-free electrodes have higher volumetric energy densities than electrodes with conductive and adhesive additives. However, most of traditional LiMe_xO_y cathodes generally share poor electrical conductivity and require substantial carbonous coatings or additives[14-15]. As well, binders and current collectors (usually Cu or Al foil) are needed for lithium batteries.

Conventional cathodes requires 30-50% volume (10wt%) filling by carbon particles and 4-6wt % binder to obtain sufficient electrical conductivity and mechanical stability,[16-17] which lead to a decrease of volumetric energy density than the theoretical value and a cost increase of 20-25%. To enhance the volumetric density and lower the cost, it is critical that the minimum volume of carbon and organic binder are used, and free-standing film would be an appropriate choice.[18] $\text{VO}_2(\text{B})$, one of the attractive materials for lithium batteries, has been synthesized by various methods.[19-23] We synthesized metastable monoclinic $\text{VO}_2(\text{B})$ nanobelts by a convenient and controllable approach in previous work.[24]

These nanobelts can be either prepared as stable colloidal solutions or self-assembled into the “paper form” films only after suction filtration. $\text{VO}_2(\text{B})$ nanobelt films are expected to afford advanced performances over conventional cathodes. This is because of the advantages of $\text{VO}_2(\text{B})$ nanobelts: First, $\text{VO}_2(\text{B})$ nanobelt is a semimetal material, so it is expected that carbon black is not needed. Little amount of binders are needed for the $\text{VO}_2(\text{B})$ nanobelt cathode as well, since the belts can easily intertwine to paper-like film. Second, the film is flexible, arising from the flexibility of original nanobelt, thus is potential for application in ultra-thin flexible batteries. Third, the improved transport of charge and diffusion of Li ions due to the nanostructured nature of one dimensional metal oxides (high surface-to-volume ratio, excellent surface activities, short diffusion path lengths for ions, and crystallographic orientation) could provide improved power density of the cathode.[25-27] Moreover, it is well known that the size and morphology of the nanomaterials are critical for the performance. The operating properties of batteries depend not only on the structure, but also on the morphology of the electrode components.[28] Therefore, the different size may make a difference on the electrochemical performance of the three samples.

Herein, we reported a free-standing $\text{VO}_2(\text{B})$ nanobelt films as additive-free cathode for lithium ion batteries. $\text{VO}_2(\text{B})$ nanobelts with different size were prepared to produce the film cathodes and the size effect on the electrochemical performance was discussed, thus enables the optimal belts size for use in cathodes materials to be chosen.

It was shown that the initial capacity was 219.4 mAh/g at current rate 10mA/g is achieved by the $\text{VO}_2(\text{B})$ nanobelt films, with an obvious voltage plateau during charge and discharge around 2.5 V. Comparable good cycling performance was also observed. In view of good conductivity, controllable morphology and flexibility of $\text{VO}_2(\text{B})$ nanobelts film, it is believed that results described here may open up another way for design of novel nanostructured materials for ultra-thin soft batteries applications.

2. EXPERIMENTAL SECTION

2.1. Sample Synthesis.

VO₂(B) nanobelts were prepared by the hydrothermal method using NH₄VO₃ and HCOOH with different concentrations. In a typical synthesis, 0.234g (2mmol) NH₄VO₃ was dispersed in 20ml deionized water under vigorous magnetic stirring to form a straw yellow solution. In order to improve the solubility, the deionized water was heated to about 40 °C firstly. Appropriate formic acid was added then, with the color of the solution changing into salmon pink immediately. The amount of formic acid added were 280µl, 440µl, and 600µl, (corresponding to pH value of 2.9, 2.7 and 2.5) with sample code VO₂(B)-I, VO₂(B)-II and VO₂(B)-III, respectively. Then the resultant solution was transferred to a 40ml autoclave and kept in an oven at 180 °C for 2 days. When the autoclaves cooled down to room temperature naturally, the product was collected via vacuum filtration. The dispersion was filtrated through a filter paper in a Buchner funnel and washed with deionized water for several times, forming a thin VO₂(B) mat. After that, the resultant mat was dried in an oven at 60 °C for 6 h and peeled off from the filter paper carefully. By this means, a flexible free-standing VO₂(B) film was obtained.

2.2. Instrument Characterization.

X-ray diffraction (XRD) data of samples were collected with a Shimadzu XRD-6000 diffractometer, using CuK α radiation ($\lambda=1.5418\text{\AA}$) at 40 kV, 30 mA. The size and morphology of as-synthesized samples were determined by scanning electron microscopy (SEM, Zeiss SUPRA 55), operated at an acceleration voltage of 5.0 kV. The samples for SEM were prepared by adhering the film onto a silicon wafer substrate.

2.3. Electrochemical Measurement.

For electrochemical evaluation, electrodes were prepared by punching the free-standing VO₂(B) films into flakes with diameter of 7 mm and dried at 120 °C in a vacuum oven for 24 h. CR2032 coin-type cells were assembled in an Ar-filled glove box using Celgard 2400 as a separator, Li foil as the counter and reference electrode, and 1M LiPF₆ EC + DEC + DMC(1:1:1 by volume) as electrolyte. All of the cells were tested galvanostatically between 1.5 and 4.0 V vs. Li/Li⁺ at a current density of 10 mA/g or 50mA/g, using a Neware automated tester.

During charging, Li was extracted from the working electrode, while during discharge, Li was inserted into the electrode.

3. RESULTS AND DISCUSSION

By controlling the addition of formic acid, which is a reducing agent and pH emollient, VO₂(B) nanobelts were easily prepared and their average aspect ratio as well as width-to-thickness ratio could

be adjusted. Free-standing $\text{VO}_2(\text{B})$ nanobelt films were then obtained by self-assembly of the as-prepared nanobelts with a filtration technology (Figure 1).

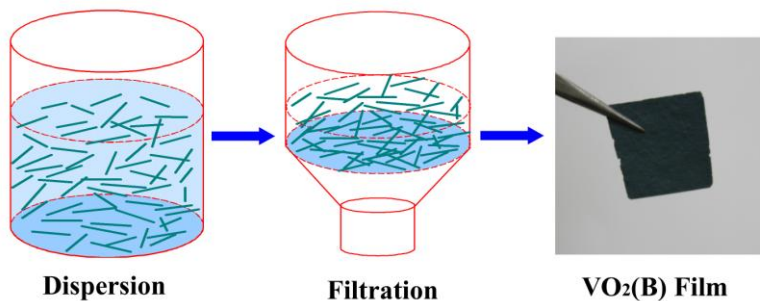


Figure 1. Scheme of the preparation of the free-standing $\text{VO}_2(\text{B})$ nanobelt films

The crystal structure and phase composition of the nanobelt film samples obtained at pH=2.9, 2.7, 2.5 (corresponding to 280 μl , 440 μl , and 600 μl formic acid) were first investigated by XRD.

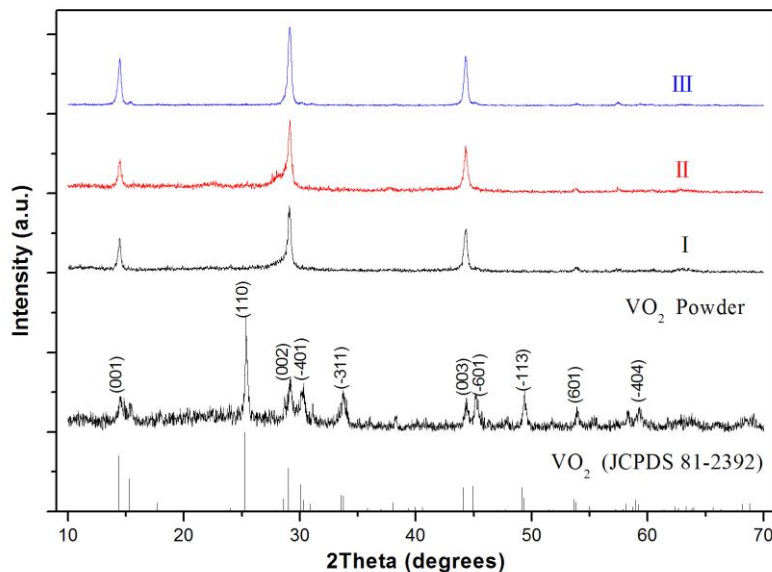


Figure 2. X-ray diffraction (XRD) patterns of free-standing $\text{VO}_2(\text{B})$ films I, II, III and powder sample of $\text{VO}_2(\text{B})$ -III.

Figure 2 shows the typical XRD patterns of the three free-standing $\text{VO}_2(\text{B})$ nanobelt films and $\text{VO}_2(\text{B})$ powder. The sharp and strong peaks of the films are indexed to $(00l)$ reflections for layered phases of $\text{VO}_2(\text{B})$, which corresponds to high oriented assembly and high crystallinity of the nanobelts. The layer spacing of the phase is determined to be 6.12 Å from the (001) reflection. To confirm the phase composition further, the film samples were ground into powder thoroughly. All the peaks of the XRD pattern of powder samples are in good agreement with the monoclinic $\text{VO}_2(\text{B})$ phase (space

group: C2/m) with lattice constants of $a = 12.09 \text{ \AA}$, $b = 3.702 \text{ \AA}$, $c=6.433 \text{ \AA}$, and $\beta= 106.6^\circ$ (JCPDS 81-2392), as shown in Figure 2, taking $\text{VO}_2(\text{B})\text{-III}$ as an example. Obviously, no other phases or impurities were observed.

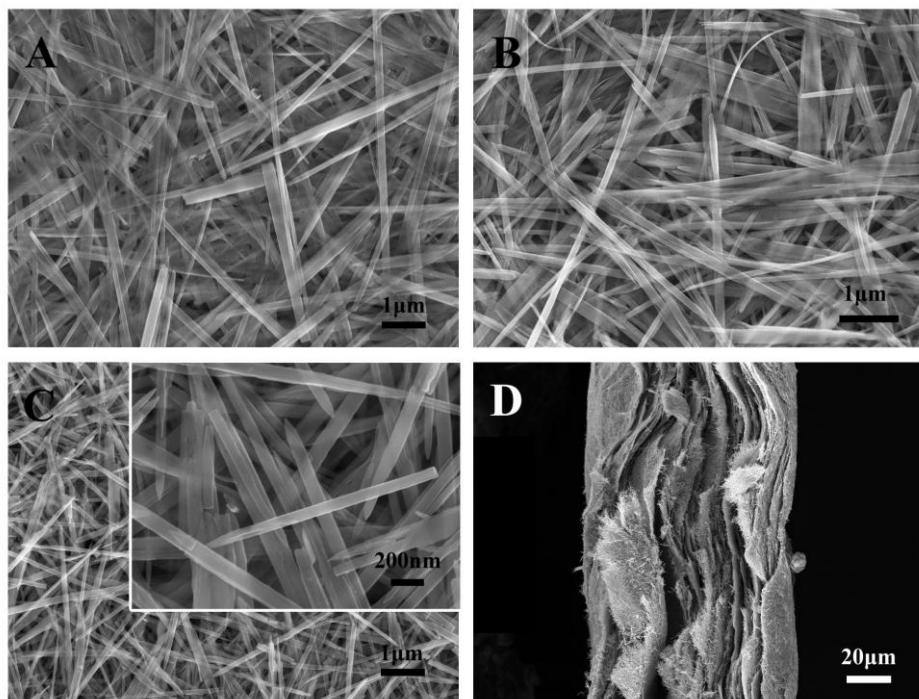


Figure 3. SEM images of top view of $\text{VO}_2(\text{B})$ film. (A) $\text{VO}_2(\text{B})\text{-I}$; (B) $\text{VO}_2(\text{B})\text{-II}$; (C) $\text{VO}_2(\text{B})\text{-III}$. A higher magnification image is shown in the inset. (D) SEM cross-sectional image of the $\text{VO}_2(\text{B})\text{-II}$ film, showing the thickness of the film is about $100\mu\text{m}$.

SEM and TEM were carried out to characterize the surface morphologies of the products. Figure 3 displays the typical SEM images of $\text{VO}_2(\text{B})$ nanobelts films. It can be seen that $\text{VO}_2(\text{B})$ nanobelts self-assembled into film during filtration. The film obtained at $\text{pH}=2.9$ ($\text{VO}_2(\text{B})\text{-I}$) contains the nanobelts with an average width of 140 nm and a length of $>10 \mu\text{m}$ (Figure 3A). When pH value decreased to 2.7 and 2.5 ($\text{VO}_2(\text{B})\text{-II}$ and III), the average width gradually reduced to 120 and 90 nm . As well, the average length decreased to about $7 \mu\text{m}$ and $3\mu\text{m}$, respectively, as shown in Figure 3B and C. It is worth mentioning that part of the $\text{VO}_2(\text{B})$ nanobelts were broken off during the process of filtration, especially in $\text{VO}_2(\text{B})\text{-I}$. As a result, sometimes it is difficult to observe the whole morphology of single $\text{VO}_2(\text{B})$ nanobelt using SEM. The cross-sectional view of the VO_2 film is displayed in Figure 3D.

The thickness of the films is about $100\mu\text{m}$. It is well acknowledged that the properties of nanoscale materials differ from the properties of individual atom, molecule, and bulk matter. 1D nanostructures are more prone to charge transport than bulk crystalline structures. Different morphologies of the same substance may also lead to different properties. Therefore, the different size of $\text{VO}_2(\text{B})$ nanobelts might contribute to different electrochemical performance.

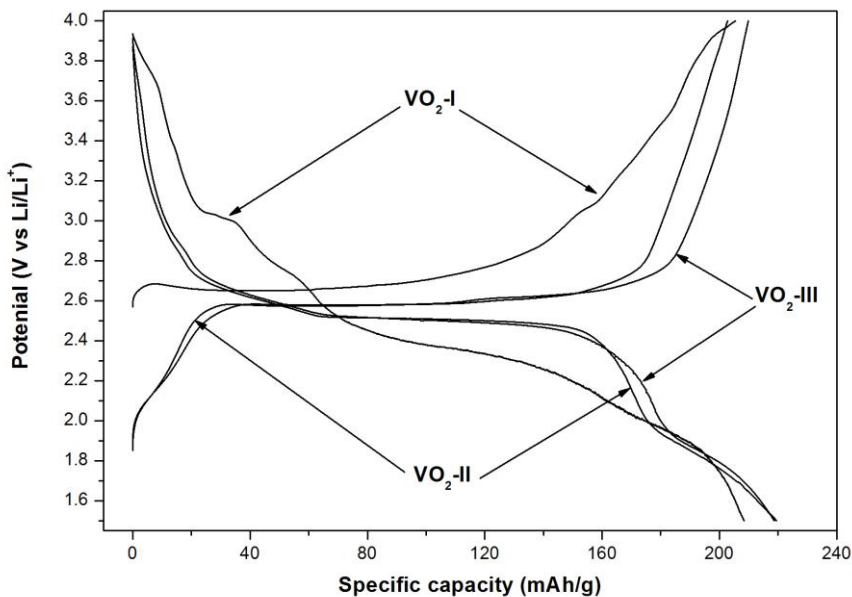


Figure 4. Initial charge and discharge voltage curves of the three samples at current density of 10mA/g.

Figure 4 shows the initial charge and discharge voltage curves of the three samples with different sizes at a rate of 10 mA/g. Sample VO₂(B)-I did not show any distinct voltage plateau, while sample VO₂(B)-II and VO₂(B)-III exhibited obvious voltage plateaus during charge and discharge around 2.5 V. Such a clear voltage plateau was seldom reported in previous work.[23, 29-33] Sample VO₂(B)-I showed first discharge and charge capacities of 208.4 and 205.5 mAh/g, that is, a coulombic efficiency of 98.6%. However, VO₂(B)-II, with capacities of 219.4 and 204.7 mAh/g, demonstrated a coulombic efficiency of 93.3%. In the case of VO₂(B)-III, the corresponding coulombic efficiency is 95.9%, with discharge and charge capacities of 218.7 and 209.8 mAh/g, respectively. Obviously, the mechanisms of the lithium intercalation in VO₂(B) crystal lattice of above two types, with or without plateau, are different. The discharge curve of sample VO₂(B)-I indicates a solid-solution lithiation mechanism. Li ions move into VO₂(B) crystal lattice gradually, forming Li_xVO₂ solid solution. Generally, reversible capacities of VO₂(B) were obtained in the range of 4 to 1V vs. Li⁺/Li through this solid solution mechanism.[21] On the other hand, the voltage plateaus of sample VO₂(B)-II and III suggest two-phase reaction during charge and discharge around 2.5 V. The voltage plateau contains ca. 160mAh/g (50% of the theoretical capacity) in the first cycle, corresponding to the formation of Li_{0.5}VO₂ phase. The overall cell reaction for the lithium insertion/deinsertion reaction in VO₂ electrode can be described as:



It has been reported that Li_xVO₂(B) could accommodate 0.5 Li/V above 2.0 V at room temperature, while further intercalation can be obtained only at higher temperatures as in kinetic, the second step is very slow [34]. VO₂(B) lattice has two different types of square pyramidal sites, 0.5 of

each per formula unit. It is thus considered that the plateau formed because the Li ion is easy to insert into one type of the sites to form a metastable phase $\text{Li}_{0.5}\text{VO}_2$, while the insertion of Li^+ greater than $x=0.5$ (into another site) would result in strong Li–Li interaction in the lattice. On the right side of the plateau, there is a slope, corresponding to a solid solution mechanism (Figure 4). Although Li insertion into $\text{VO}_2(\text{B})$ becomes more and more difficult, Li can still be inserted into the surface of the materials as a result of the high specific surface area of $\text{VO}_2(\text{B})$ nanobelts. From the discharge curve of $\text{VO}_2(\text{B})$ -II and III, we can see that the plateaus trend to get longer with the decrease of the nanobelts size, due to the higher specific surface area. After 10 cycles, the reversible discharge capacities were 158.9, 176.3, and 155.6 mAh/g, which were greater than 70% of the initial discharge capacity. When the scan rate increased to 50 mA/g, the first discharge capacity decreased to 153.8, 201.3, and 175.9 mAh/g. Actually, with a higher current density, the capacity becomes smaller, and the plateau becomes shorter and less flat. The irreversible capacity is firstly closely related to the poor electronic conductivity of $\text{Li}_x\text{VO}_2(\text{B})$. It was reported that the electronic conductivity of $\text{Li}_{0.5}\text{VO}_2(\text{B})$ is only 1/100 of that of $\text{VO}_2(\text{B})$ [35]. That causes lithium extraction-insertion become irreversible due to dynamics at high current density. The second reason for deterioration in cycling performance can be attributed to electrochemical corrosion of lithium anode. As it is known, the internal resistance caused by interfacial resistance of lithium anode will increase with current density.

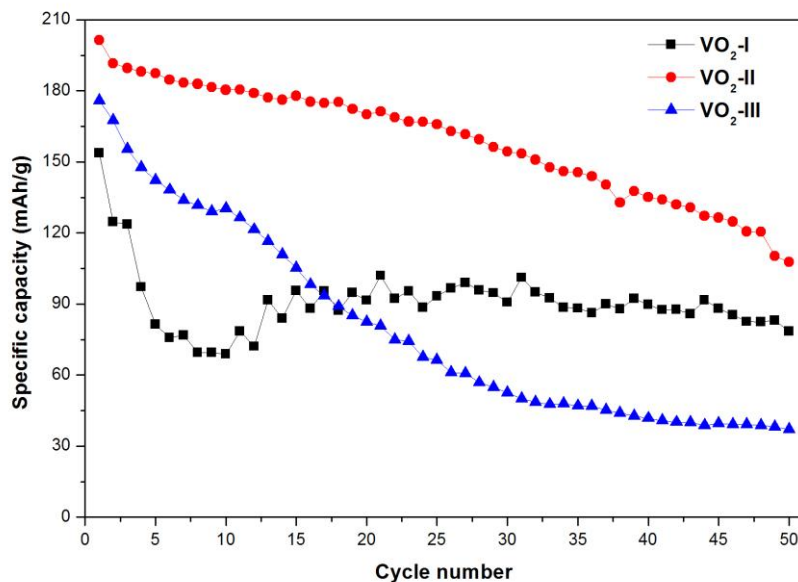


Figure 5. The cycling behavior comparison of the three samples at a scan rate of 50mA/g.

As reported, VO_2 with various morphologies could hardly exhibit good cyclability.[29, 33] Specific capacity irreversibly fades quickly due to the electrodes side reaction and structural transformation. Though batteries with nanoscale materials deliver more power quickly with less heat, an increase in undesirable electrode/electrolyte reactions leads to self-discharge, poor cycling and calendar life [36] It remains a great challenge to improve the cycling performance of VO_2 for chemists

and material scientists. Figure 5 shows the specific capacity retention of the three samples up to 50 cycles at current density of 50 mA/g. Obviously, sample VO₂(B)-II is superior to the other two samples. The first discharge capacity of VO₂(B)-II was 201.3 mAh/g, and the capacity faded gradually to 107.7 mAh/g in 50 cycles. However, a significant irreversibility was observed on VO₂(B)-I for the first 10 cycles and the capacity faded quickly from 153.8 to 68.9 mAh/g. Quite surprisingly, after this initial drop, the capacity rose slowly during the next ten cycles to reach a maximum of about 100 mAh/g and turned completely reversible over the subsequent cycles. For the sample VO₂(B)-III, the capacity decreased from 175.9 to 37.0 mAh/g directly. The capacity retentions were 44.8, 53.5, and 21.0%, after 50 cycles. With the increasing cycle number, lower and lower discharge curves were observed. That is, the charge and discharge trend to be more and more difficult, since the layer structure might have been destructed to yield low energy level substance and less Li can be intercalated in the layer. Therefore, the discharge capacity becomes smaller involuntarily.

Why did the three films prepared by nanobelts with different sizes show significantly different electrochemical behavior? The structure and morphology of the VO₂(B) electrodes after prolonged cycling were examined by XRD and SEM.

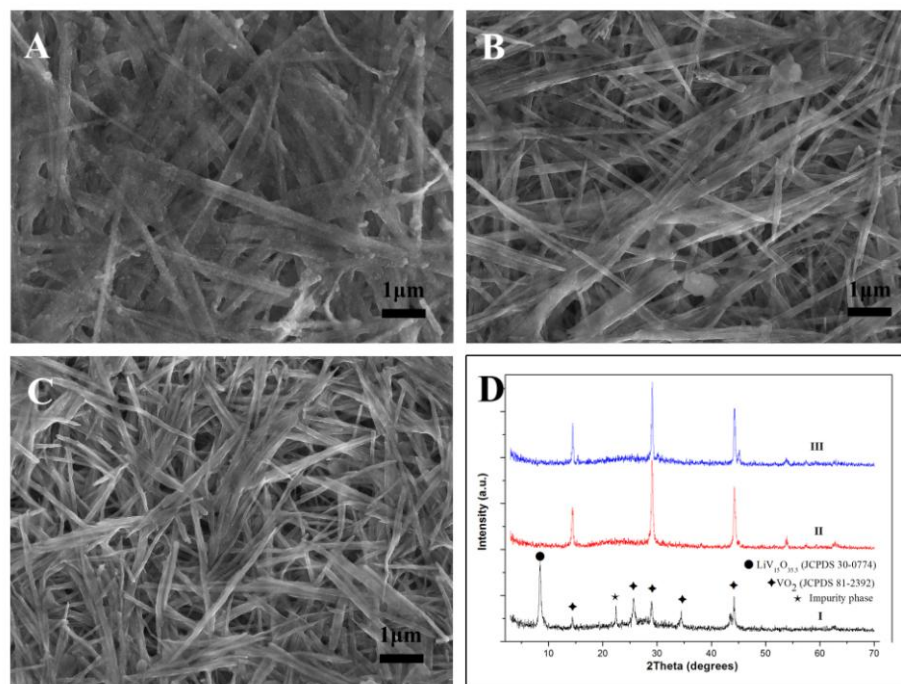


Figure 6. SEM and XRD images of the three films after 50 cycles. (A) VO₂(B)-I; (B) VO₂(B)-II; (C) VO₂(B)-III. (D) XRD pattern.

Figure 6A-C shows SEM images of the three different VO₂(B) electrodes after 50 full electrochemical lithiation/delithiation cycles. In general, for all those three electrodes, the morphology and the mechanical integrity are still retained, being a proof of their good mechanical stability. However, it is observed that there are small particles formed on the surface of the tested sample

$\text{VO}_2(\text{B})$ -I (Figure 6A). As mentioned above, the insertion and extraction of Li^+ in $\text{VO}_2(\text{B})$ -I undergo a solid-solution mechanism. During the process, lithium ion insertion causes volume expansion, even crystal restructure and the material pulverization. Since the pulverization is beyond retrievable, the structure of the electrode was break up and form amorphous or nanocrystalline phase in the cycle test. The XRD characterization of the sample after 50 cycles is in reasonable agreement with this phenomenon. As can be noticed in Figure 6D, additional peaks consistent with the $\text{VO}_2(\text{B})$ powder and $\text{LiV}_{15}\text{O}_{35.5}$ (JCPDS 30-0774) appeared in the XRD pattern of sample $\text{VO}_2(\text{B})$ -I, which demonstrates the partial loss of the epitaxial nature of the belts due to their swelling and pulverization and new phase of $\text{LiV}_{15}\text{O}_{35.5}$ formation in the electrochemical cycles. After the pulverization, part of the active substance did not participate in electrochemical Li insertion as a result of inferior electrical contact. This is the reason why sample $\text{VO}_2(\text{B})$ -I faded quickly in initial several cycles. The following increase in capacity in the 20th cycle indicates that some kinetics limitations are gradually reduced during battery operation, which might result from the relaxation of the new structure to create smooth pathway for the lithium ions insertion and extractions.[21, 30, 37] The better performance of sample II and III should attribute to the smaller size of the nanobelts, which provide improved charge transport and Li ions diffusion and avoid the structure cracking during cell operation. This is confirmed by XRD analysis. Seen from Figure 6D, the XRD patterns of sample II and III after electrochemical test remain unchanged. Moreover, nanoscale materials have high specific surface area and high surface Gibbs free energy, it is thereby easier to form agglomerated state. As a result, the frequent capacity fading was observed in nano-sized materials for lithium batteries, consistent with the situations for sample II and III. The increased specific surface area and thus the higher surface energy of the $\text{VO}_2(\text{B})$ -III nanobelts with smaller size enhance the interface reaction between the electrode and electrolyte and the formation of agglomerated state, resulting in capacity fading more quickly (Figure 5). This is also verified by the SEM characterization, in which the structure recombination and amalgamation of sample III is more significant. Therefore, considering that the decrease in particle size yields increase in capacity values, a balance should be controlled in order to avoid parasite reactions with the electrolyte. Further structure studies are required to better understand the fundamentals of lithium insertion into these $\text{VO}_2(\text{B})$ phases.

4. CONCLUSION

In summary, free-standing $\text{VO}_2(\text{B})$ nanobelt films were prepared as additive-free cathode for lithium ion batteries, via self-assembly of $\text{VO}_2(\text{B})$ nanobelt with a filtration technology. The $\text{VO}_2(\text{B})$ nanobelts with different sizes were synthesized with a simple hydrothermal method by controlling the amount of formic acid addition. XRD and SEM characterization indicated high crystallinity and good morphology of the nanobelts. Comparable electrochemical performance was observed by electrochemical analysis, in particular considering our electrodes are free-standing and additive-free. However, the long-term cyclability of $\text{VO}_2(\text{B})$ still need to be improved when taking into account its practical application. The connection between the electrochemical performance and structure transformation has been discussed in detail. The results also demonstrated the influence of morphology

on the electrochemical properties of the VO₂(B) nanobelts. Considering the different size of the three samples, three could be an optimized value to achieve the optimum electrochemical performance.

ACKNOWLEDGEMENT

This work is supported by the NSFC (grand No.20901046 and 20801058), the State Key Project of Fundamental Research for Nanoscience and Nanotechnology (Grant No. 2011CB935902), the Beijing Natural Science Foundation (Grant No.2102033) and the Program for New Century Excellent Talents in Universities.

References

1. L.-F. Cui, L. Hu, J.W. Choi and Y. Cui, *ACS Nano*, 4 (2010) 3671-3678
2. P.G. Bruce, S. Bruno and T. Jean-Marie, *Angew. Chem. Int. Ed.*, 47 (2008) 2930-2946.
3. M. Armand and J.M. Tarascon, *Nature*, 451 (2008) 652-657.
4. Z. Tao, J. Liang and J. Chen, *Chem. Mater.*, 20 (2007) 667-681.
5. J.M. Tarascon and M. Armand, *Nature*, 414 (2001) 359-367.
6. R. Santhanam, B. Rambabu, *Int. J. Electrochem. Sci.*, 4 (2009) 1770-1778.
7. VS Reddy Channu, Rudolf Holze, Edwin H. Walker Jr., S.A. Wicker Sr, Rajamohan R. Kalluru, Quinton L. Williams, Wilbur Walters, *Int. J. Electrochem. Sci.*, 5 (2010) 1355-1366.
8. J.S. Zhao, L. Wang, X. M. He, C. R. Wan, C. Y. Jiang, *Int. J. Electrochem. Sci.*, 5 (2010) 478-488.
9. N. Kim, M. Chung and I. Park, *Electrode of ultra thin manganese battery and manufacturing method therefor*. 2005, Google Patents.
10. R.P. Raffaelle, B.J. Landi, J.D. Harris, S.G. Bailey and A.F. Hepp, *Mater. Sci. Eng., B*, 116 (2005) 233-243.
11. A.L.M. Reddy, M.M. Shaijumon, S.R. Gowda and P.M. Ajayan, *Nano Lett.*, 9 (2009) 1002-1006.
12. H. Zhang, G. Cao, Z. Wang, Y. Yang, Z. Shi and Z. Gu, *Nano Lett.*, 8 (2008) 2664-2668.
13. V.L. Pushparaj, M.M. Shaijumon, A. Kumar, S. Murugesan, L. Ci, R. Vajtai, R.J. Linhardt, O. Nalamasu and P.M. Ajayan, *Proc. Natl. Acad. Sci.*, 104 (2007) 13574-13577.
14. Sung-Keun Kim, Woon-Tae Jeong, Hong-Ki Lee, Joongpyo Shim, *Int. J. Electrochem. Sci.*, 3 (2008) 1504-1511.
15. P. Kalyani, *Int. J. Electrochem. Sci.*, 4 (2009) 30-42.
16. L. Wang, J.S. Zhao, S.H. Guo, X.M. He, C.Y. Jiang and C.R. Wan, *Int. J. Electrochem. Sci.*, 5 (2010) 1113-1126.
17. X.Y. Cao, L.J. Guo, J.P. Liu and L.L. Xie, *Int. J. Electrochem. Sci.*, 6 (2011) 270-278.
18. M.S. Whittingham, *Chem. Rev.*, 104 (2004) 4271-4302.
19. C. Wu, J. Dai, X. Zhang, J. Yang, F. Qi, C. Gao and Y. Xie, *Angew. Chem.*, 122 (2010) 138-141.
20. Z. Gui, R. Fan, W.Q. Mo, X.H. Chen, L. Yang, S.Y. Zhang, Y. Hu, Z.Z. Wang and W.C. Fan, *Chem. Mater.*, 14 (2002) 5053-5056.
21. C. Tsang and A. Manthiram, *J. Electrochem. Soc.*, 144 (1997) 520-524.
22. W. Li, J.R. Dahn and D.S. Wainwright, *Science*, 264 (1994) 1115-1118.
23. A.M. Kannan and A. Manthiram, *Solid State Ionics*, 159 (2003) 265-271.
24. J.F. Liu, Q.H. Li, T.H. Wang, D.P. Yu and Y.D. Li, *Angew. Chem. Int. Ed.*, 43 (2004) 5048-5052.
25. S.W. Lee, B.-S. Kim, S. Chen, Y. Shao-Horn and P.T. Hammond, *J. Am. Chem. Soc.*, 131 (2009) 671-679.
26. Y.-H. Kao, W.C. Carter and Y.-M. Chiang, *Chem. Mater.*, 22 (2009) 1088-1097.
27. R. Ma, Y. Bando, L. Zhang and T. Sasaki, *Adv. Mater.*, 16 (2004) 918-922.
28. W.U. Huynh, J.J. Dittmer and A.P. Alivisatos, *Science*, 295 (2002) 2425-2427.
29. S. Zhang, Y. Li, C. Wu, F. Zheng and Y. Xie, *J. Phys. Chem. C*, 113 (2009) 15058-15067.

30. H. Liu, Y. Wang, K. Wang, E. Hosono and H. Zhou, *J. Mater. Chem.*, 19 (2009) 2835-2840.
31. C. Wu, Z. Hu, W. Wang, M. Zhang, J. Yang and Y. Xie, *Chem. Commun.*, 2008, 3891-3893.
32. R. Li and C.-Y. Liu, *Mater. Res. Bull.*, 45 (2010) 688-692.
33. Z. Chen, S. Gao, L. Jiang, M. Wei and K. Wei, *Mater. Chem. Phys.*, 121 (2010) 254-258.
34. B. Zachau-Christiansen, K. West and T. Jacobsen, *Mater. Res. Bull.*, 20 (1985) 485-492.
35. D. Aurbach, A. Nimerger, B. Markovsky, E. Levi, E. Sominski and A. Gedanken, *Chem. Mater.*, 14 (2002) 4155-4163.
36. A.S. Arico, P. Bruce, B. Scrosati, J.-M. Tarascon and W. van Schalkwijk, *Nat. Mater.*, 4 (2005) 366-377.
37. J. Kim and A. Manthiram, *Nature*, 390 (1997) 265-267